

# Monitoring Reversible Tight Junction Modulation with a Current-Driven Organic Electrochemical Transistor

Katharina Lieberth, Maximilian Brückner, Fabrizio Torricelli, Volker Mailänder, Paschalis Gkoupidenis, and Paul W. M. Blom\*

The barrier functionality of a cell layer regulates the passage of nutrients into the blood. Modulating the barrier functionality by external chemical agents like poly-L-lysine (PLL) is crucial for drug delivery. The ability of a cell layer to impede the passage of ions through it and therefore to act as a barrier, can be assessed electrically by measuring the resistance across the cell layer. Here, an organic electrochemical transistor (OECT) is used in a current-driven configuration for the evaluation of reversible modulation of tight junctions in Caco-2 cells over time. Exposure to low and medium concentrations of PLL initiates reversible modulation, whereas a too high concentration induces an irreversible barrier disruption due to nonfunctional tight junction proteins. The results demonstrate the suitability of OECTs to in situ monitor temporal barrier modulation and recovery, which can offer valuable information for drug delivery applications.

## 1. Introduction

In the human body, barrier tissues play an essential role by selectively controlling the transport of nutrients, ions, or drugs across the barrier. Human tissue layers are categorized into endothelial and epithelial cell lines.<sup>[1]</sup> Endothelial cells separate blood as well as lymphatic vessels from tissue, whereas the epithelial cells separate inner organs from the blood veins. Barrier tissues exhibit various tightness, according to their


functionality.<sup>[2]</sup> The selective transport of drugs across the barrier takes place either through the cells (transcellular) or in between the cells (paracellular).<sup>[3,4]</sup> Understanding of these processes is essential for in vitro testing of effective drug delivery.<sup>[2]</sup> For oral drug delivery, Caco-2 cells, having an intermediate barrier functionality,<sup>[1]</sup> are well studied as a model for the gastrointestinal tract.<sup>[5]</sup> Intercellular tight junctions (TJ) play a predominant role for paracellular permeability<sup>[6]</sup> between the apical, exposed to lumen, and the basolateral surface domain, exposed to lamina.<sup>[6,7]</sup> As shown in **Figure 1a**, the paracellular barrier consists of TJs, adherent junctions, and desmosomes.<sup>[8]</sup> TJ complexes are protein complexes including occludin,<sup>[9]</sup> claudin,<sup>[8]</sup> zonulin,<sup>[10,11]</sup> and cytoplasmic proteins.<sup>[12]</sup> TJ complexes are crucial to maintain barrier integrity. They are dynamically modulated by the intracellular signaling transduction system and a number of extracellular stimuli enabling the passage of nutrients and restricting harmful substances.<sup>[10,11,13]</sup> TJ modulation regulates the paracellular pathway via transient opening by TJ modulators having a direct or indirect effect on TJs.<sup>[4,7,14]</sup> Since the early 90s, polycations such as chitosan or poly-L-lysine (PLL) are known to be potential promoters of drug delivery across intestinal barrier tissues.<sup>[15,16]</sup> Polycations represent the most convenient manner to affect oral bioavailability having attributes such as enhancing drug solubility, protecting sensitive drugs from rapid degradation due to positive charges at a broad pH range, and serving as a permeability enhancer.<sup>[17]</sup> PLL modulates the barrier functionality of epithelial cell layers by enhancing paracellular permeability as a TJ modulator.<sup>[15,18,19]</sup> Monitoring the effect of PLL on the paracellular permeability through cell layers with barrier function has been first studied by McEwan et al. (1993), investigating the potential difference of physical barriers, such as MDCK canine kidney cells, with the Ussing-chamber.<sup>[15]</sup> The work of Roblendo et al. (1999) investigated the effect of PLL on BEAS-2B human bronchial cells by measuring the radioactivity<sup>[14C]</sup> mannitol flux.<sup>[18]</sup> As the most related work, Ranaldi et al. (2002) investigated the increase of paracellular permeability of Caco-2 cells during a 2 h exposure to PLL concentration-dependent using TEER measurements.<sup>[19]</sup> However, there is no study to our knowledge on in situ monitoring reversible TJ modulation with PLL as modulator. An opening of TJs causes a temporary loss of barrier functionality and allows the passage of ions or drugs across the barrier, respectively.<sup>[4,8]</sup> Furthermore, it has been demonstrated that

K. Lieberth, M. Brückner, Prof. V. Mailänder, Dr. P. Gkoupidenis, Prof. P. W. M. Blom

Max Planck Institute for Polymer Research  
Ackermannweg 10, Mainz 55128, Germany  
E-mail: blom@mpip-mainz.mpg.de

M. Brückner, Prof. V. Mailänder  
Dermatology Clinic  
University Medical Center of the Johannes Gutenberg-University Mainz  
Langenbeckstr. 1, Mainz 55131, Germany

Dr. F. Torricelli  
Department of Information Engineering  
University of Brescia  
Via Branze 38, Brescia 25123, Italy

 The ORCID identification number(s) for the author(s) of this article can be found under <https://doi.org/10.1002/admt.202000940>.

© 2021 The Authors. Advanced Materials Technologies published by Wiley-VCH GmbH. This is an open access article under the terms of the Creative Commons Attribution-NonCommercial-NoDerivs License, which permits use and distribution in any medium, provided the original work is properly cited, the use is non-commercial and no modifications or adaptations are made.

DOI: 10.1002/admt.202000940

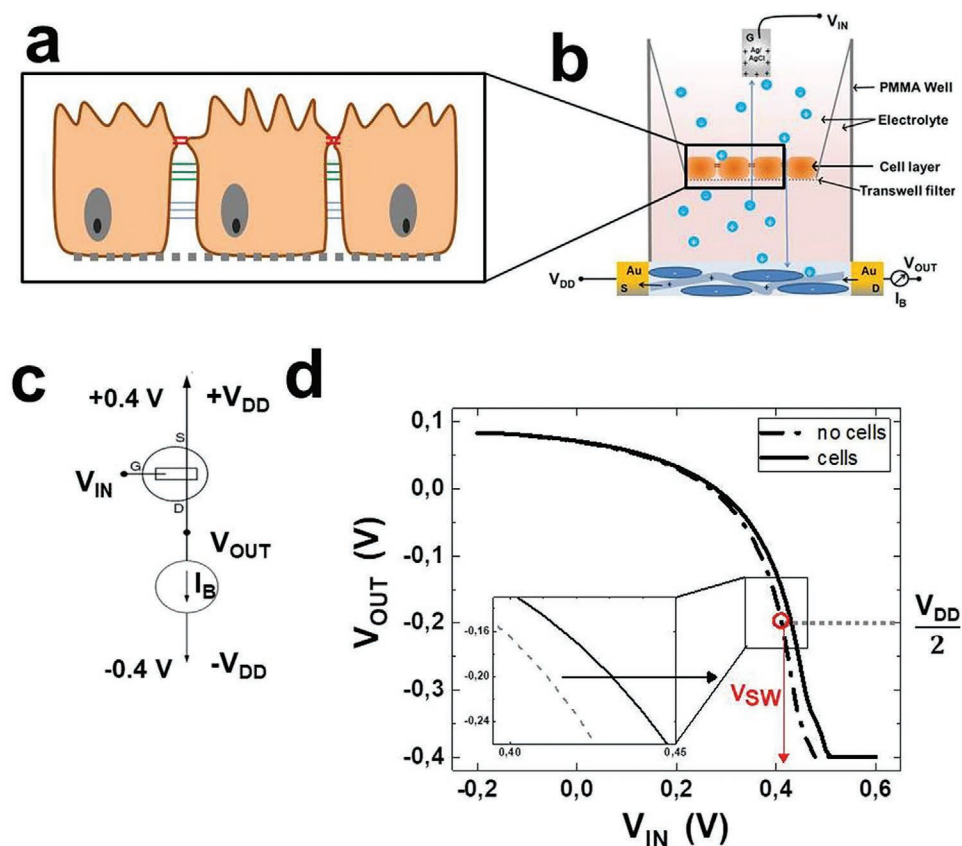


**Figure 1.** Current-driven OEET with cell barrier integrity. a) Scheme of epithelial cell layer that functions as a physical barrier facilitated by intercellular TJs. The paracellular barrier consists of TJs (red), adherent junctions (green), and desmosomes (blue). b) Scheme of the OEET device structure with an integrated Transwell filter in presence of cell layers as barrier tissue with TJs in between the cells (red lines). PEDOT:PSS as the active area between the gold electrodes, source (S) and drain (D), defines the OEET's geometries:  $W = 2 \text{ mm}$ ,  $L = 1 \text{ mm}$ ,  $t = 100 \text{ nm}$ . An Ag/AgCl gate electrode (G) and the cell culture medium EMEM is utilized as an electrolyte. Mobile ionic charge carriers are labeled in bright blue, nonmobile PSS<sup>-</sup> anions in dark blue and holes in black. c) Schematic electronic circuit of a current-driven OEET. d) Measured  $(V_{\text{OUT}} - V_{\text{IN}})$ -transfer characteristics of a current-driven OEET in absence (dashed line) and presence (solid line) of barrier tissue.  $V_{\text{SW}}$  (red circle) is defined as a specific  $V_{\text{IN}}$  (red arrow) at which  $V_{\text{OUT}}$  is equal to half  $|V_{\text{DD}}|$ , marked as a horizontal grey dashed line to guide the eye. For this experiment Caco-2 cells were seeded on a Transwell filter (1.12 cm<sup>2</sup>, poresize: 0.4  $\mu\text{m}$ ) and measured on day 14.

PLL induces reversible TJ modulation through morphological modifications of the F-actin cytoskeleton as well as a redistribution of zonulin and occludin.<sup>[19]</sup> Therefore, recording temporal TJ modulation under the influence of a polycationic modulator is of great importance to assess the transient state of barrier functionality with potential applications in drug delivery.

To detect modulation of TJ properties, imaging techniques like immunofluorescence spectroscopy or the permeability assay have been commonly utilized.<sup>[20]</sup> However, due to their invasiveness along with a low temporal resolution, alternative methods are highly wanted. As a quantitative parameter, the trans-epithelial electrical resistance (TEER) defines the barrier functionality of the cell layer indicating TJ modulation.<sup>[2,12,21]</sup> One possibility of quantification is to measure the TEER by using a volt-ohm-meter.<sup>[22,23]</sup> This set-up, measuring paracellular conductance, consists of a basal electrode, centered on the bottom of the electrolyte containing chamber, and a top electrode placed on the lid. The latter one is dipped into the apical electrolyte, held by a Transwell-filter, which has a permeable filter enabling free-standing cell culture.<sup>[23]</sup> This method is easy to handle, but suffers from low reproducibility and low

temporal resolution.<sup>[21]</sup> Measuring frequency-dependent impedance with electrochemical impedance spectroscopy (EIS) is more advanced and has higher reproducibility as compared to TEER. But EIS has a low time resolution,<sup>[24,25]</sup> whereas commercial EIS set-ups enable to scan several cell layers on Transwell filters in parallel in an automated approach.<sup>[25]</sup>

In recent years, the organic electrochemical transistor (OEET) became an alternative attractive means to electrically assess barrier tissue properties.<sup>[26,27]</sup> An OEET is a transistor where the conducting channel, typically consisting of poly(3,4-ethylenedioxythiophene): polystyrene sulfonate (PEDOT:PSS), is in direct contact with an aqueous electrolyte in which a gate electrode is placed.<sup>[28]</sup> When a positive gate voltage is applied, cations permeate into the channel and dedope the PEDOT:PSS material by compensating the negative PSS anions, leading to a decrease of the drain current. Thus, the OEET is an ion-to-electron transducer.<sup>[29]</sup> As ions penetrate into the bulk of the channel, the channel capacitance is volumetric leading to a very high transconductance.<sup>[30]</sup> Over the last years, the OEET has received raising interest in the field of bioelectronics,<sup>[26,29,31]</sup> with applications covering neural interfacing,<sup>[32]</sup> analyte detection,<sup>[31]</sup>

neuromorphics,<sup>[33]</sup> electronic plants<sup>[34]</sup> as well as sensing the barrier integrity of barrier tissues.<sup>[35]</sup> Regarding the latter, TJ opening or irreversible disruption with, e.g., hydrogen peroxide, ethanol, EGTA, Salmonella or Forskolin, a CFTR agonist, has been monitored by transient response measurements.<sup>[21,26,36,37]</sup> OECTs have been also utilized for EIS-based cell sensing.<sup>[36,38]</sup> More recently, the sensitivity of OECTs to ions has been strongly enhanced at low voltages using the OECT in a current-driven, inverter-like configuration.<sup>[39]</sup> Because of this enhanced sensitivity, minute changes of ionic concentrations can be detected and therefore also small changes of a biological barrier can be monitored. Furthermore, the enhanced sensitivity allows the acquisition of only one output characteristic at an effective frequency (determined by the voltage sweep rate) as compared to more traditional methods, where, e.g., the transconductance is measured across a frequency range, which is more time-consuming. An investigation on irreversible barrier tissue disruption with hydrogen peroxide using a current-driven OECT confirmed the improved ion sensitivity compared to transient response measurements.<sup>[40]</sup> Therefore, a current-driven OECT is an attractive alternative to electrically monitor in real-time the reversible opening and closing of TJs, which is of great importance for drug delivery.

Here, we study the epithelial barrier tissue integrity under the influence of PLL as TJ modulator with a current-driven OECT. The electrical response of the barrier tissue is measured as a function of TJ modulator concentration. For low and medium concentration, the results demonstrate a reversible modulation of barrier functionality, whereas an irreversible effect is observed for high concentration. To obtain more insight in the TJ modulation mechanism, immunofluorescence imaging is performed focusing on the displacement of occludin, as a relevant TJ protein. Combining electrical OECT measurements and fluorescence imaging, it is postulated that PLL creates an opening of TJs by redistributing occludin, which is in accordance to literature.<sup>[19]</sup>

## 2. The Current-Driven OECT: Sensing Reversible Tight Junction Modulation

### 2.1. The Current-Driven OECT: An Impedance Sensor for Barrier Tissue

The device structure of an OECT with an integrated Transwell filter containing a cell layer is schematically indicated in Figure 1b. The active area of the PEDOT:PSS channel has a width of 2 mm and length of 1 mm between gold source and drain electrodes. A detailed description of the fabrication process is presented in the experimental section. The basal electrolyte was confined by a polymethylmethacrylate (PMMA-) well glued on the glass substrate. The cell culture medium EMEM was utilized as basal and apical electrolyte. Cells were seeded on a Transwell filter (cell seeding is described in detail at the Experimental Section). In brief, cells were incubated for 14 d until reaching a TEER of  $\approx 400 \Omega \text{ cm}^2$ , before being integrated in the device structure, to ensure a functional barrier created by a dense cell layer. On the apical side, an Ag/AgCl pellet was immersed in the electrolyte functioning as gate electrode. The electronic circuit of a current-driven OECT is schematically portrayed in Figure 1c.<sup>[39]</sup> To perform such measurements, the

voltage at the gate (input voltage,  $V_{IN}$ ) was altered, whereas the output voltage,  $V_{OUT}$  was detected at the drain. As the current-driven OECT is highly ion sensitive, the measurements were performed at a specific frequency. In order to create an inverter-like circuit topology with the OECT, a direct current was applied at the drain, labeled as current bias  $I_B$ , controlling the threshold voltage. The supply voltage  $\pm V_{DD}$  defines the saturation level of the  $(V_{OUT} - V_{IN})$ -transfer characteristics, and was set by means of voltage compliance at the current-generator.<sup>[41]</sup> The current-driven OECT functions as an ionic sensor, investigating the alteration of TJ properties of the Caco-2 cell layer under the influence of PLL. An effective barrier tissue with pristine TJs has a low paracellular ion permeability. Because PLL induces TJ-opening, the ion permeability increases temporarily. Due to the gate potential, ions then pass the barrier tissue, and permeate into the PEDOT:PSS channel. The OECT transduces the presence of ions into an electronic signal. All  $(V_{OUT} - V_{IN})$ -measurements were performed at  $I_B = [0.2; 0.5] \text{ mA}$  and  $V_{DD} = |0.4| \text{ V}$  with 15 min delay time under physiological conditions. The  $(V_{OUT} - V_{IN})$ -transfer characteristics of the current-driven OECT with an integrated cell layer monitoring ion permeability across a cell layer is displayed in Figure 1d. To analyze the cell barrier modifications, the shifting of  $(V_{OUT} - V_{IN})$ -transfer characteristics were quantified by the switching voltage  $V_{SW}$ , indicated in Figure 1d.  $V_{SW}$  is the minimum  $V_{IN}$  required to operate the OECT in saturation. Effectively, this circuit topology represents an inverter circuit. For example, when  $V_{IN}$  is scanned from negative to positive voltages, there is a transition in  $V_{OUT}$  between  $+V_{DD}$  and  $-V_{DD}$ . In this transition  $V_{SW}$  expresses the gate voltage at which there is the onset of the saturation regime of the transistor.  $V_{SW}$  is defined to be at  $V_{OUT} = 1/2(-V_{DD})$ .<sup>[39]</sup> Hence, the  $(V_{OUT} - V_{IN})$ -transfer characteristic in presence of the integrated cell layer (black) results in a higher  $V_{SW}$  compared to a device in absence of barrier tissue (grey, dashed), as seen in Figure 1d. Being able to monitor minute changes in ionic concentration makes the current-driven OECT a beneficial and competing method to evaluate cell barrier integrity and its TJ modulation.

### 2.2. Sensing Reversible Tight Junction Modulation

Schematically, the four experimental steps to sense reversible TJ modulation with a current-driven OECT are represented in Figure 2a. Once  $V_{IN}$  was applied to the device with an integrated plain Transwell filter, cations from the apical and basal side were injected into the channel without facing any cell barrier at the Transwell filter, presented in sketch (1). Since, at a given  $V_{IN}$  many ions can penetrate into the PEDOT:PSS channel, rapid dedoping leads to a decrease of  $V_{OUT}$  until saturation was reached (Figure 1d dashed line). When an intact cell layer is introduced, the transport of ions into the channel is impeded by the TJs, shown in sketch (2). Therefore, a higher value of  $V_{IN}$  is needed to dedope the PEDOT:PSS channel, such that the  $(V_{OUT} - V_{IN})$ -transfer characteristics shift to the right. Upon opening of the TJs during PLL exposure (sketch (3)), the ion flow to the channel is restored, and the  $(V_{OUT} - V_{IN})$ -transfer characteristics shift back to the left (lower  $V_{IN}$ ). Finally, after exchanging the electrolyte and the time of recovery of TJs (sketch (4)) the  $(V_{OUT} - V_{IN})$ -transfer characteristics shift

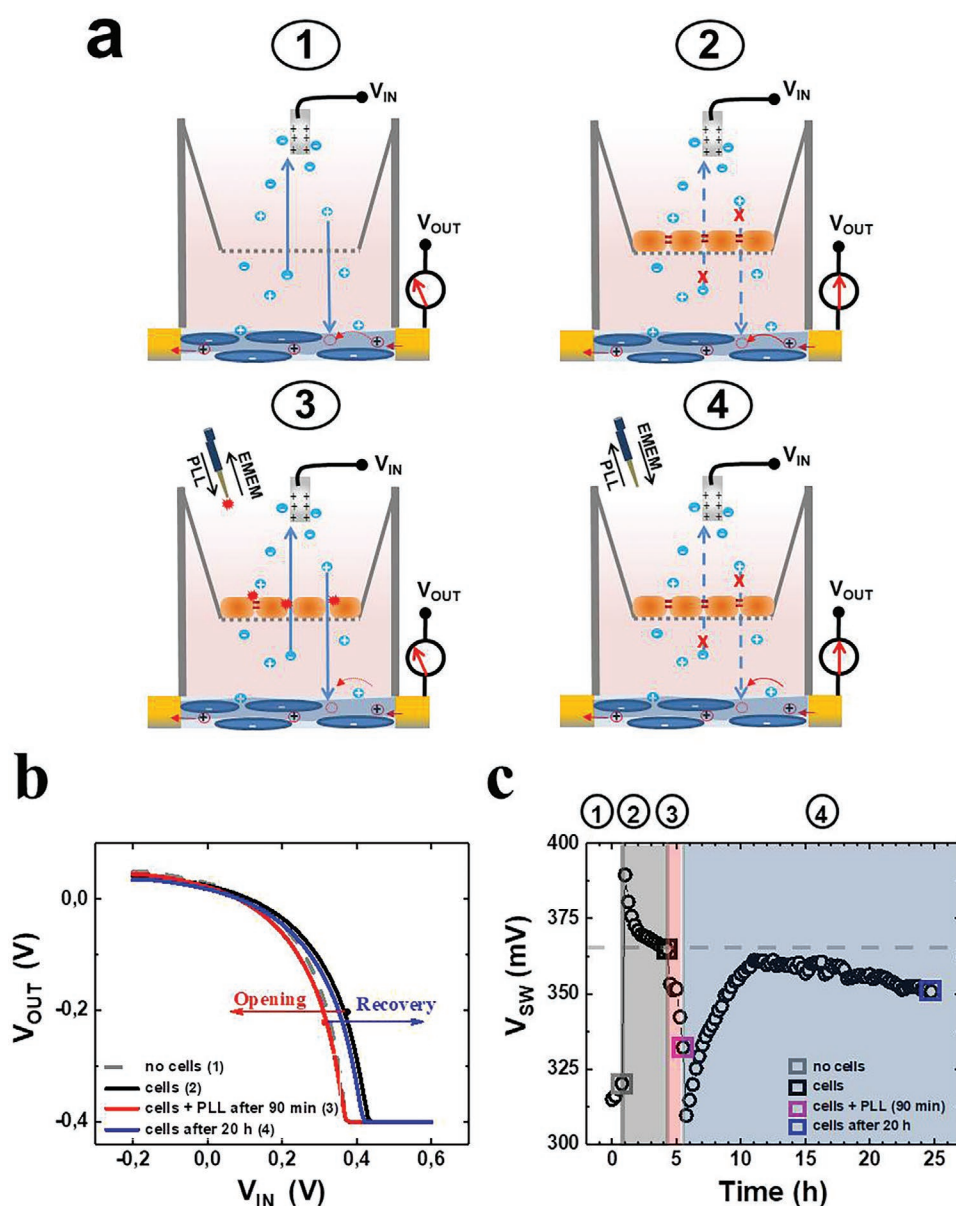


**Figure 2.** Sensing reversible tight junction modulation over time with a current-driven OECT: a) Schematic of the four experimental steps performed under physiological conditions: The device with an integrated Transwell filter in absence (1) and in presence (2) of a Caco-2 cell layer; The barrier functionality of the integrated cell layer is symbolized by TJ's (red). Addition of PLL, while keeping the electrolyte volume constant (3); Incubation after exchanging electrolyte apical and basal (4); The barrier functionality of the integrated cell layer is symbolized by TJ's (yellow). b)  $(V_{OUT} - V_{IN})$ -Transfer characteristics of a current-driven OECT at  $I_B = 0.5$  mA and  $V_{DD} = -0.4$  V. Selected  $(V_{OUT} - V_{IN})$ -transfer characteristics of the OECT in absence (grey dashed, 1) and presence (black, 2) of the barrier tissue, 90 min after adding PLL (red, 3) and 20 h after exchanging the electrolyte (blue, 4). c) Monitoring the extracted  $V_{SW}$  of all measured  $(V_{OUT} - V_{IN})$ -transfer characteristics over time of the experiment. Vertical grey lines help to distinguish experimental steps. Horizontal grey dashed lines indicate  $V_{SW}$  of an intact barrier tissue. The OECT's geometries were  $W = 2$  mm,  $L = 1$  mm,  $t = 100$  nm. Ag/AgCl was utilized as gate electrode and EMEM as an electrolyte. For this experiment Caco-2 cells were seeded on a Transwell filter ( $1.12$  cm<sup>2</sup>, poresize:  $0.4$   $\mu$ m) and measured on day 14.

back towards the situation of the closed membrane. Figure 2b represents the  $(V_{OUT} - V_{IN})$ -transfer characteristics of all four experimental steps. The left shift caused by the opening of TJ's during PLL exposure gives rise to a decay of  $V_{SW}$ , whereas a right shift of the  $(V_{OUT} - V_{IN})$ -transfer characteristics due to recovery of the TJ's leads to a resumption of  $V_{SW}$ . In Figure 2c,  $V_{SW}$  is monitored over the time of the experiment. To assure

device stability,  $(V_{OUT} - V_{IN})$ -transfer characteristics were measured over 1 h prior to cell layer integrity. Then a Transwell filter with an integrated cell layer replaced the plain Transwell filter, shown in sketch (2).  $V_{SW}$  increased of  $\approx 45$  mV, as the Caco-2 cell layer acted as a barrier for ions, shown in Figure 2c. For each sample the  $(V_{OUT} - V_{IN})$ -transfer characteristics of the integrated cell layer with intact barriers were measured over 3 h to



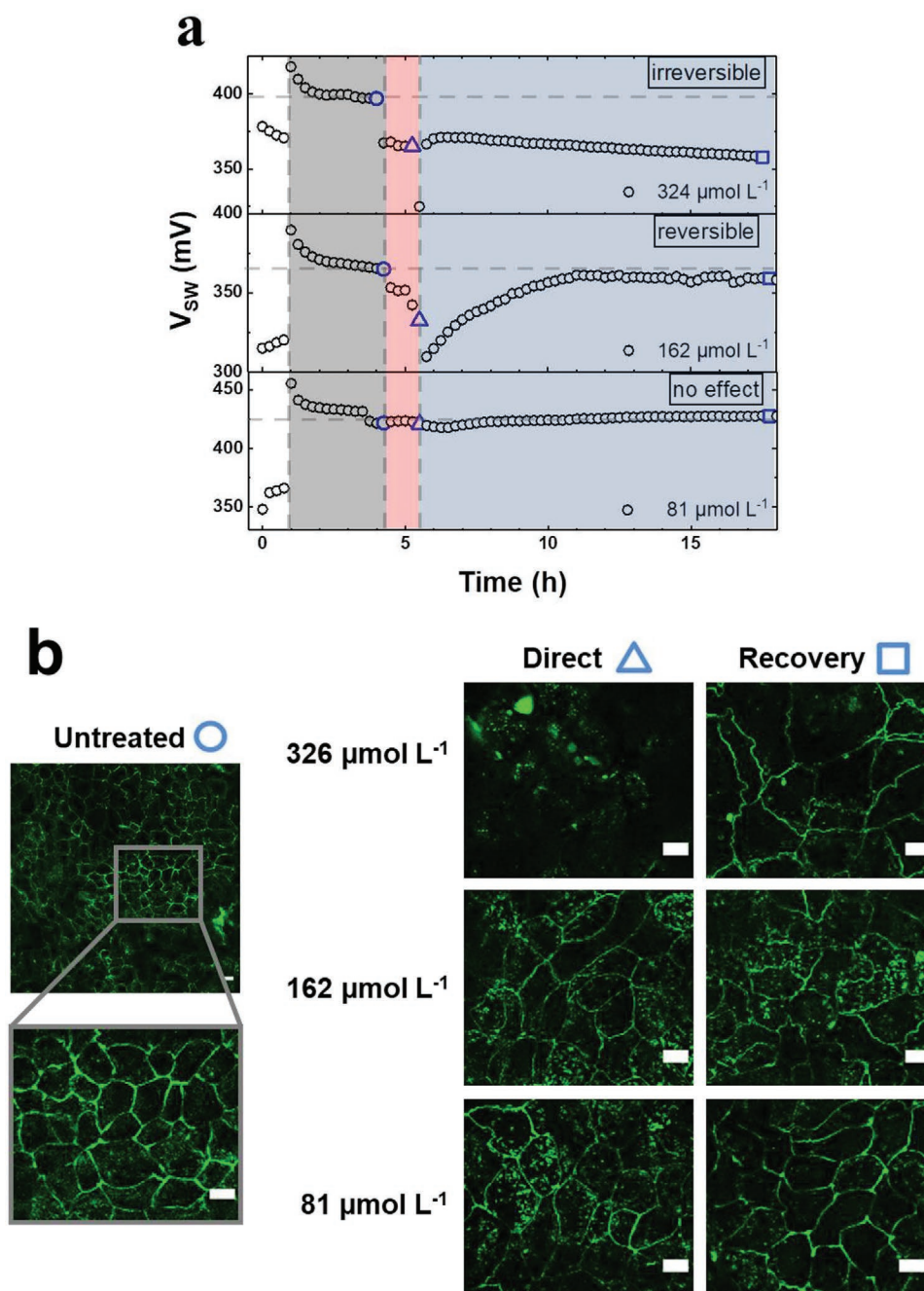


**Figure 3.** The concentration effect of TJ modulator PLL measured by current-driven OECT as a dynamic sensor for reversible tight junction modulation: a)  $V_{sw}$  over time of the experiment for three different concentrations of PLL ( $81, 162, 324 \times 10^{-6}$  M). Horizontal grey dashed lines indicate  $V_{sw}$  of an intact barrier tissue. Vertical grey dashed lines help to distinguish experimental steps. The OECTs geometries were  $W = 2$  mm,  $L = 1$  mm,  $t = 100$  nm. Ag/AgCl was utilized as gate electrode and EMEM as electrolyte. For this experiment Caco-2 cells were seeded on a Transwell filter ( $1.12$  cm<sup>2</sup>, poresize:  $0.4$   $\mu$ m) and measured on day 14. b) Immunostaining of occludin (green) in human CaCo-2 cells cultivated on day 14 on coverslips ( $1.12$  cm<sup>2</sup> and treated with different amounts of PLL (see visualization of occludin after PLL exposure (direct) and recovery in the experimental section for a detailed description). All scale bars represent  $10$   $\mu$ m.

assure stable barrier functionality. As demonstrated in Figure S1 (Supporting Information), the stable barrier functionality was provided over 24 h, implicating device stability. When PLL was added in a medium concentration of  $162 \times 10^{-6}$  M apical to the electrolyte, the volume was kept constant. We observe that 90 min after PLL exposure  $V_{sw}$  decayed to the level of the

Transwell filter without cells. This demonstrates that the cell layer lost its barrier functionality indicating TJ opening. As a result of a subsequent exchange of the electrolyte apical and basal,  $V_{sw}$  resumed over 6 h almost to the level of the intact barrier with an increase of  $\approx 41$  mV. The comeback of more than 90% of its initial barrier functionality indicates a recovery of TJs. To

sum up, reversible barrier modulation and more specifically TJ modulation was monitored with the OECT in current-driven mode. We observe that the TJ opening occurs fast, whereas the recovery of the TJs is rather slow.

### 2.3. Sensing Tight Junction Modulation as a Function of Concentration

Figure 3a represents  $V_{SW}$  of ( $V_{OUT} - V_{IN}$ )-transfer characteristics measured with a current-driven OECT over time for various PLL concentrations. To investigate the concentration effect of PLL as TJ modulator on the cell barrier integrity, three concentrations have been tested:  $81 \times 10^{-6}$  M (small),  $162 \times 10^{-6}$  M (medium), and  $324 \times 10^{-6}$  M (high). In the example for low PLL concentration,  $V_{SW}$  increased by  $\approx 55$  mV when inserting a cell layer into the device set-up. The effect of a low PLL-concentration resulted in only a few mV change in  $V_{SW}$ , as the barrier function is lost only slightly. Hence, the addition of a low PLL concentration had practically no effect on TJ modulation. After the exchange of electrolyte, a steady increase in  $V_{SW}$  overcoming the level of the intact cell barrier is observed. By adding a medium PLL concentration ( $162 \times 10^{-6}$  M), the effect was far more pronounced, as already presented in Figure 2b. Therefore, PLL in medium concentration served as a reversible TJ modulator. In contrast, upon adding a high PLL concentration ( $324 \times 10^{-6}$  M),  $V_{SW}$  decreased directly by  $\approx 40$  mV to the reference response in absence of the cell layer and remained constant during and after the exposure. Hence, the effect of high PLL concentration had an irreversible effect on the cell barrier. The relatively fast opening of the TJs observed with the OECT is attributed to a displacement of proteins like occludin and zonulin.<sup>[19]</sup> The recovery of the TJs is rather slow, as it requires the transport of occludin and zonulin to the cell membrane. Already Yu et al. and McEwan et al. have shown reversible permeability enhancement of PLL in a concentration from 5 to  $100 \mu\text{g mL}^{-1}$  exposed to kidney epithelium (MDCK I).<sup>[15,42]</sup> For the bronchial epithelium (BEAS-2B), it was found that after 1 h exposure to  $0.2\text{--}10 \mu\text{g mL}^{-1}$  PLL, a full recovery of barrier function is maintained after 12 h. Barrier modulation is assumed to be caused by spontaneous transformations in intercellular junctions and cell proliferation.<sup>[18]</sup> Recently, the effect of PLL in the concentrations 0.01% and 0.001% to urothelium was investigated exhibiting reversible TJ modulation. For Caco-2 cells, it is assumed that a recovery after PLL treatment is much faster as compared to Chitosan.<sup>[19]</sup> The application of PLL in drug delivery as a permeability enhancer is reported to be successful.<sup>[43]</sup> Deionized water as solvent of PLL is affecting the osmotic pressure of the cell layer, but the effect of pure solvent was minor to the one seen upon the exposure to PLL, portrayed in Figure S2 in the Supporting Information. Also, an investigation of the cytotoxicity on Caco-2 cells exposed to PLL in four different concentrations over three different time durations is displayed in Figure S3 in the Supporting Information. It resumed that a small or medium concentration of PLL dissolved in water was not affecting the cell metabolism during the exposure time of the experiment, whereas the cell viability decays to  $\approx 50\%$  in case of exposure to a high concentration of PLL.

In order to visualize the effect of PLL on Caco-2 cell barriers as measured with the current-driven OECT, additional immunofluorescent antibody labeling was performed to visualize TJ modulation by confocal laser scanning microscopy (cLSM). For this reason, the Caco-2 cells were exposed to PLL under similar conditions compared to the current-driven OECT (see Experimental Section for a detailed experimental description). The transmembrane protein occludin was immunocytochemically stained to highlight the effect on the TJ barrier integrity directly after PLL exposure, compared to staining after an incubation time of 20 h subsequent PLL exposure (Figure 3b). Regarding imaging directly after PLL exposure, samples under exposure of small and medium PLL concentrations ( $81$  and  $162 \mu\text{mol L}^{-1}$ ) show almost no difference in the staining pattern of occludin compared to the untreated Caco-2 cells. However, the drop in resistance for a medium PLL concentration effect, monitored by a large alteration in  $V_{SW}$  with the current-driven OECT (Figure 3a), is not visible in the occludin staining. It should be noted that conformational changes in the TJs occur on the nm scale, which are hard to resolve with a microscope. This shows that electrophysiological investigations of TJ modulation can have an advantage over microscopy. Regarding images 20 h after exchanging the electrolyte, occludin staining is fully visible, which is in agreement with the reversible effect measured with the current-driven OECT. However, occludin staining directly after a high PLL treatment ( $326 \mu\text{mol L}^{-1}$ ) is clearly impaired. Here, the characteristic junctional organization of occludin is completely disrupted and reorganized into the intracellular compartments. Interestingly, subsequent to an incubation over 20 h after electrolyte exchange, the occludin staining is almost completely visible again. Therefore, when we combine the electrophysiological investigations with the visualization of TJ modulation, we conclude that the occludin proteins steadily reassemble during the 20 h recovery at the outer cell membranes. However, they either lose their functional properties of firmly sealing the adjacent cells or are not able to fully close all junctional cell connections, resulting in the inability of not being able to restore the initially measured barrier function. This effect can be seen both on Caco-2 cells grown on coverslips as well as on cells grown on Transwell filters (Figure S4, Supporting Information). In addition, investigating the recovery behavior of Caco-2 cells after PLL exposure in more detail, cell viability studies show that after an exposure to high PLL concentration, the cells are no longer metabolically active, leading to an increase in cytotoxicity (Figure S5, Supporting Information). As a result, tight junction proteins like occludin might still be present at their physiological site; however, they are not functional anymore because also the cells are not viable.

### 3. Conclusion

In conclusion, reversible TJ modulation has been detected with an OECT in current-driven configuration by investigating paracellular permeability across an epithelial cell barrier. It was demonstrated that a small PLL concentration is hardly affecting TJ properties, whereas a medium PLL concentration induces reversible TJ modulation. In contrast, a high PLL concentration causes irreversible alteration of TJ properties. With the

OECT in current-driven configuration not only the process of TJ opening, but also of TJ closing can be precisely monitored as a variation of the output voltage. The work shows the progress of OECT technology towards in vitro testing of TJs for clinical applications as drug targeting and screening.

## 4. Experimental Section

**Device Fabrication:** Glass slides were cleaned by sonication first in water with soap (Micro-90) and then in a 1:1 vol/vol solvent mixture (acetone, isopropanol), followed by drying and UV ozone cleaning. Source and drain gold contacts were thermally evaporated using a shadow mask defining the active area ( $W = 2$  mm,  $L = 1$  mm). An adhesion layer of chromium (5 nm) was previously deposited. The PEDOT:PSS formulation consisted of an aqueous dispersion of the conducting p-type polymer PEDOT:PSS (Clevis PH1000, 90 vol.%), one droplet of the surfactant Zonyl (Du Pont FSO-100) and the conductivity enhancer dimethyl sulfoxide (DMSO, 10 vol.%). The dispersion of PEDOT:PSS was spin coated on the device defining the layer thickness of  $\approx 100$  nm. After annealing of 1 h at  $140$  °C the devices were rinsed with DI water for swelling of the active area. A PMMA-well was placed on top for a defined volume of the electrolyte, using double-sided tape to prevent leakage.

**Cell Culture:** Caco-2 cells (DSMZ, ACC 169) were seeded at  $1.5 \times 10^5$  cells/insert ( $1.12$  cm<sup>2</sup>, pore size =  $0.4$   $\mu$ m). The area of the Transwell-filter was reduced from  $1.12$  cm<sup>2</sup> to  $\approx 0.08$  cm<sup>2</sup> by coating PDMS on the back side for the filter. The PDMS-modified Transwell filters were coated with collagen as stated in the literature for enhanced cell attachment.<sup>[44]</sup> Cells were cultured in EMEM (Eagle's Minimum Essential Medium, Invitrogen) with 10% FBS (fetal bovine serum, Invitrogen),  $2 \times 10^{-3}$  M glutamine (GlutaMax-1, 100 $\times$ , Invitrogen) and Pen-strep (10 000  $\mu$ g mL<sup>-1</sup> penicillin, 10 000  $\mu$ g mL<sup>-1</sup> streptomycin, Invitrogen) with a medium change every 2 or 3 d.<sup>[44]</sup> Cells were maintained at  $37$  °C in a humidified atmosphere with 5% CO<sub>2</sub> during cell culturing and the experiment.

**Caco-2 Cell Exposure to PLL in Transwell Filter:** Experiments were performed on day 14 after seeding, corresponding to a TER of  $\approx 400$   $\Omega$  cm<sup>2</sup>.<sup>[45,40]</sup> The TER was measured with a handheld Volt-Ohm meter EVOM2 from World Precision Instruments. Before adding poly-L-lysine (PLL) in DI water ( $0.56 \times 10^{-6}$  M,  $M_w = 30$ – $70$  kDa, Sigma Aldrich) apical to the cell layer, the same volume of electrolyte was removed before to keep the ionic concentration similar. Cell layers were exposed to the following three concentrations of PLL:  $81 \times 10^{-6}$  M added in a volume of  $72$   $\mu$ L ( $\Delta V = 14\%$ );  $162 \times 10^{-6}$  M added in a volume of  $120$   $\mu$ L ( $\Delta V = 24\%$ );  $324 \times 10^{-6}$  M added in a volume of  $240$   $\mu$ L ( $\Delta V = 48\%$ ). After 90 min of treatment the electrolyte was exchanged apical and basal. During the whole experiment the samples were kept in a humidified atmosphere with 5% CO<sub>2</sub>.

**Visualization of Occludin after PLL Exposure and Recovery:** Confocal laser scanning microscopic images (cLSM) of immunofluorescently stained Caco-2 cells against the TJ protein occludin confirmed the presence of TJs and TJ opening over 90 min of PLL exposure followed by 20 h of recovery in EMEM cell culture medium supplemented with 10% FBS.

The Caco-2 experiments were performed at two different time points and under two different conditions of cultivation. At day 14, untreated cells ( $n = 2$  wells), cells with  $81$   $\mu$ mol L<sup>-1</sup> PLL ( $n = 1$  well), cells with  $162$   $\mu$ mol L<sup>-1</sup> PLL ( $n = 1$  well), and cells with  $326$   $\mu$ mol L<sup>-1</sup> PLL ( $n = 3$  wells), were tested in  $\mu$ -Slide 8 well chambered coverslips (ibidi) for both the direct and the recovery approach (Figure 3b), as well as in Corning FluoroBlok Transwells filters ( $0.3$  cm<sup>2</sup>, pore size =  $3.0$   $\mu$ m) (Figure S4, Supporting Information) ( $n = 2$  wells, Caco-2 cells treated with  $326$   $\mu$ mol L<sup>-1</sup> recovery approach only), showing same results as on coverslips. At day 21, untreated cells ( $n = 1$  well), cells with  $81$   $\mu$ mol L<sup>-1</sup> PLL ( $n = 1$  well), cells with  $162$   $\mu$ mol L<sup>-1</sup> PLL ( $n = 2$  wells), and cells with  $326$   $\mu$ mol L<sup>-1</sup> PLL ( $n = 3$  wells), were tested in  $\mu$ -Slide 8 well chambered coverslips (ibidi) for the recovery approach.

For the experimental procedure, cells were cultivated on collagen precoated coverslips for 14 d and for 21 d or on Corning FluoroBlok

Transwell filters for 14 d (Figure S4, Supporting Information). As no significant difference in the results of cells on day 14 and day 21 was observed, only the results of cells on day 14 are presented in this work.

After PLL exposure (diluted in cell culture medium supplemented with 10% FBS), the cells were washed once with Dulbecco's phosphate buffered saline (PBS) and then fixed with 4% paraformaldehyde in PBS for 10 min at room temperature, followed by permeabilization with 0.2% Triton-X 100 and 1% BSA in PBS for 2 h. Milli-Q water (Merck) and 20% DMSO in cell culture medium were used as controls. Staining was performed with an occludin monoclonal antibody (AF488, Thermo 33–1511) with a concentration of  $5$   $\mu$ g mL<sup>-1</sup> in  $0.15$  mL PBS for each  $\mu$ -Slide 8 well and in  $0.25$  mL PBS for each Corning FluoroBlok Transwell filter for 24 h at  $4$  °C in the fridge. After antibody incubation, the occludin dilution in PBS was removed and the cells were washed with PBS. For the Transwell filters, the cell-containing membranes were excised carefully with a scalpel and placed with the cells facing upwards on a glass slide. Fluoromount-G mounting medium was added to the top of the cells and a cover slip was used to seal the construct. Z-stack images were taken on the LSM SP5 STED Leica Laser Scanning Confocal Microscope (Leica, Germany), composed of an inverse fluorescence microscope DMI 6000CS equipped with a multilaser combination using a HCX IRAPO L 25.0  $\times$  0.95 water objective. The specimen's FITC dye was excited with the excitation laser at  $488$  nm and detected with an emission filter at  $510$ – $550$  nm. Editing of images was conducted by using the Fiji software and Microsoft Power Point. In Fiji, the z-stacks were converted to 2D by using the maximum intensity projection. The occludin channel was pseudo-colored in green. In addition, the Fiji adjust function was used to automatically correct brightness and contrast. Finally, Fiji selected images were processed by Microsoft Power Point adjusting the brightness (+20%) and contrast (+40 %).

**Cell Viability Assay:** Caco-2 cells were seeded in a 96-well plate (Greiner Bio-One, Austria), instead of Transwell filters, with a cell number of  $5 \times 10^3$  cells per well in  $100$   $\mu$ L.<sup>[46]</sup> After four days of cultivation at  $37$  °C and 5% CO<sub>2</sub>, the medium was removed. Poly-L-lysine dilutions ( $81.4$ ,  $162.86$ ,  $325.7$ , and  $570$   $\mu$ mol L<sup>-1</sup>) were prepared in 10% FBS supplemented EMEM (except for  $570$   $\mu$ mol L<sup>-1</sup>, which was used directly) and added in a volume of  $100$   $\mu$ L to the cells. Samples were handled in biological triplicates. Caco-2 cells were incubated at  $37$  °C and 5% CO<sub>2</sub> for 1, 2, and 4 h before conducting the viability assay. In case of the cell recovery, Caco-2 cells were incubated for 90 min with poly-L-lysine dilutions followed by a recovery of 20 h in fresh EMEM medium (10% FBS) before conducting the viability assay. Milli-Q water and 20% DMSO in medium were used as positive controls. CellTiter-Glo Luminescent Cell Viability Assay (Promega, Germany) was performed according to the manufacturer's instructions. The luminescence signal was measured with an Infinite M1000 plate reader (Tecan, Switzerland).

**OECT Operation:** All electrical measurements were performed in a humidified atmosphere with 5% CO<sub>2</sub> by using a Keithley 4200-Semiconductor Characterization System and were analyzed by using OriginLab software. Cell culture medium (EMEM) was utilized as an electrolyte apical and basal. A Ag/AgCl electrode (pellet, 2 mm, Warner Instruments) operated as a gate, immersed in the Transwell filter. The operating gate voltage was kept well below  $1.0$  V to avoid water electrolysis and any cell damage. The experiment was performed in a continuous measurement to minimize initialization parameter variations. Before integrating a Transwell filter with cell layer, a prototype Transwell filter in absence of a cell layer was employed to measure device stability over one hour. The device structure remained then unchanged during the entire measurement time over 23 h. The cell layer stability was proven over three hours prior to add PLL. The OECT was measured in the current-driven configuration with a supply voltage of  $V_{DD} = 0.4$  V, and a range of input voltage applied at the gate  $V_{IN}$ , was swept in a range of  $[-0.2; 0.65]$  V at a current bias  $I_B = 0.5$  mA with a step rate of  $15$  mV.

**Data Presentation:** The data is presented as one set of experiment. Additional experiments were designed for reproducibility. Among all measurements, the overall behavior (electrical characterization) was reproducible; Software: For the statistical analysis, OriginLab was used.



## Supporting Information

Supporting Information is available from the Wiley Online Library or from the author.

## Acknowledgements

Open access funding enabled and organized by Projekt DEAL.

## Conflict of Interest

The authors declare no conflict of interest.

## Data Availability Statement

The data that support the findings of this study are available from the corresponding author upon reasonable request.

## Keywords

biosensors, organic electrochemical transistor, poly-L-lysine, reversible tight junction modulation

Received: September 21, 2020

Revised: January 20, 2021

Published online: April 9, 2021

- [1] M. S. Balda, L. Gonzfilez-Mariscal, R. G. Contreras, M. Macias-Silva, M. E. Torres-Marquez, J. A. Garcia-Sainz, M. Cereijido, *J. Membr. Biol.* **1991**, 122, 193.
- [2] M. A. Deli, *Biochem. Biophys. Acta* **2009**, 1788, 892.
- [3] J. Pionte, L. Winkler, H. Wolburg, S. L. Müller, N. Zuleger, C. Piehl, B. Wiesner, G. Krause, I. E. Blasig, *FASEB J.* **2008**, 22, 146.
- [4] J. M. Anderson, C. M. van Itallie, *Curr. Biol.* **1999**, 9, R922.
- [5] F. Ingels, S. Deferme, N. Delbar, M. Oth, P. Augustijns, *J. Pharm. Belg.* **2002**, 57, 153.
- [6] A. S. Fanning, L. Mitic, J. M. Anderson, *J. Am. Soc. Nephrol.* **1999**, 10, 1337.
- [7] J. M. Anderson, M. S. Balda, A. S. Fanning, *Curr. Opin. Cell Biol.* **1993**, 5, 772.
- [8] J. M. Anderson, *Physiol.* **2001**, 16, 126.
- [9] K. Matter, M. S. Balda, *Int. Rev. Cytol.* **1999**, 1861, 117.
- [10] J. M. Anderson, B. R. Stevenson, D. A. Goodenough, M. S. Mooseker, *J. Cell Biol.* **1986**, 103, A71.
- [11] A. S. Fanning, C. M. van Itallie, J. M. Anderson, *Mol. Biol. Cell* **2012**, 23, 577.
- [12] K. Sonaje, E.-Y. Chuang, K.-J. Lin, T.-C. Yen, F.-Y. Su, M. T. Tseng, H.-W. Sung, *Mol. Pharmaceutics* **2012**, 9, 1271.
- [13] C. Chelakkot, J. Ghim, S. H. Ryu, *Exp. Mol. Med.* **2018**, 50, 1.
- [14] M. S. Balda, K. Matter, *Semin. Cell Dev. Biol.* **2000**, 11, 281.
- [15] G. T. A. McEwan, M. A. Jepson, B. H. Hirst, N. L. Simmons, *Biochem. Biophys. Acta* **1993**, 1148, 51.
- [16] a) I. Westergren, B. B. Johansson, *Acta Physiol. Scand.* **1993**, 149, 99; b) A. F. Kotzé, H. L. Luessen, B. J. de Leeuw, A. G. deBoer, J. C. Verhoef, H. E. Junginger, *J. Controlled Release* **1998**, 51, 35; c) G. Sandri, P. Poggi, M. C. Bonferoni, S. Rossi, F. Ferrari, C. Caramella, *J. Pharm. Pharmacol.* **2006**, 58, 1327.
- [17] a) C.-M. Lehr, J. A. Bouwstra, E. H. Schacht, H. E. Junginger, *Int. J. Pharm.* **1992**, 78, 43; b) M. P. Deacon, S. MCGurk, C. J. Roberts, P. M. Williams, S. J. B. Tendler, M. C. Davies, S. S. Davis, S. E. Harding, *Biochem. J.* **2000**, 348, 557.
- [18] R. F. Roblendo, M. W. D. S. Barber, *Toxicol. Sci.* **1999**, 51, 119.
- [19] G. Ranaldi, I. Marigliano, I. Vespignani, G. Perozzi, Y. Sambuy, *J. Nutr. Biochem.* **2002**, 13, 157.
- [20] a) M. Ramuz, A. Hama, M. Huerta, J. Rivnay, P. Leleux, R. M. Owens, *Adv. Mater.* **2014**, 26, 7083; b) S. Tria, L. H. Jimison, A. Hama, M. Bongo, R. M. Owens, *Biosensors* **2013**, 3, 44.
- [21] L. H. Jimison, S. A. Tria, D. Khodagholy, M. Gurfinkel, E. Lanzarini, A. Hama, G. G. Malliaras, R. M. Owens, *Adv. Mater.* **2012**, 24, 5919.
- [22] B. Srinivasan, A. R. Kolli, M. B. Esch, H. E. Abaci, M. L. Shuler, J. J. Hickman, *J. Lab. Autom.* **2015**, 20, 107.
- [23] F. Decataldo, M. Barbalinardo, M. Tessarolo, V. Vurro, M. Calienni, D. Gentili, F. Valle, M. Cavallini, B. Fraboni, *Adv. Mater. Technol.* **2019**, 4, 1900207.
- [24] a) J. Wegener, C. R. Keese, I. Giaever, *Exp. Cell Res.* **2000**, 259, 158; b) D. A. Koutsouras, L. V. Lingstedt, K. Lieberth, J. Reinholz, V. Mailänder, P. W. M. Blom, P. Gkoupidenis, *Adv. Healthcare Mater.* **2019**, 8, 1901215.
- [25] J. Wegener, D. Abrams, W. Willenbrink, H.-J. Galla, A. Janshoff, *BioTechniques* **2004**, 37, 590.
- [26] S. A. Tria, M. Ramuz, M. Huerta, P. Leleux, J. Rivnay, L. H. Jimison, A. Hama, G. G. Malliaras, R. M. Owens, *Adv. Healthcare Mater.* **2014**, 3, 1053.
- [27] S. T. Tria, L. H. Jimison, A. Hama, M. Bongo, R. M. Owens, *Biochem. Biophys. Acta* **2013**, 1830, 4381.
- [28] D. A. Bernards, G. G. Malliaras, *Adv. Funct. Mater.* **2007**, 17, 3538.
- [29] J. Rivnay, P. Leleux, M. Sessolo, D. Khodagholy, T. Hervé, M. Fioocchi, G. G. Malliaras, *Adv. Mater.* **2013**, 25, 7010.
- [30] J. Rivnay, P. Leleux, M. F. Ferro, M. Sessolo, A. Williamson, D. Koutsouras, D. Khodagholy, M. Ramuz, X. Stakos, R. M. Owens, C. Benar, J.-M. Badier, C. Bernard, G. G. Malliaras, *Sci. Adv.* **2015**, 1, e1400251.
- [31] J. Rivnay, S. Inal, A. Salleo, R. M. Owens, M. Berggren, G. G. Malliaras, *Nat. Rev. Mater.* **2018**, 3, 99.
- [32] a) D. Koutsouras, A. Hama, J. Pas, P. Gkoupidenis, B. Hivert, C. Faivre-Sarrailh, E. Pasquale, R. M. Owens, G. G. Malliaras, *MRS Commun.* **2017**, 7, 259; b) J. Pas, C. Pitsalidis, D. A. Koutsouras, P. P. Quilichini, F. Santoro, B. Cui, L. Gallais, R. P. O'Connor, G. G. Malliaras, R. M. Owens, *Adv. Biosyst.* **2018**, 2, 1700164.
- [33] a) P. Gkoupidenis, N. Schaefer, B. Garlan, G. G. Malliaras, *Adv. Mater.* **2015**, 27, 7176; b) P. Gkoupidenis, D. A. Koutsouras, G. G. Malliaras, *Nat. Commun.* **2017**, 8, 15448.
- [34] E. Stavrinidou, R. Gabrielsson, E. Gomez, X. Crispin, O. Nilsson, D. T. Simon, M. Berggren, *Sci. Adv.* **2015**, 1, e1501136.
- [35] a) N. Y. Shim, D. A. Bernards, D. J. Macaya, J. A. DeFranco, M. Nikolou, R. M. Owens, G. G. Malliaras, *Sensors* **2009**, 9, 9896; b) S. Y. Yeung, X. Gu, C. M. Tsang, S. W. G. Tsao, I. M. Hsing, *Sens. Actuators, B* **2019**, 297, 126761.
- [36] M. Ramuz, A. Hama, J. Rivnay, P. Leleux, R. M. Owens, *J. Mater. Chem. B* **2015**, 3, 5971.
- [37] a) S. A. Tria, M. Ramuz, L. H. Jimison, A. Hama, R. M. Owens, *J. Visualized Exp.* **2014**, 84, 51102; b) C. Yao, C. Xie, P. Lin, F. Yan, P. Huang, I. M. Hsing, *Adv. Mater.* **2013**, 25, 6575.
- [38] J. Rivnay, M. Ramuz, P. Leleux, A. Hama, M. Huerta, R. M. Owens, *Appl. Phys. Lett.* **2015**, 106, 8\_1.
- [39] M. Ghittorelli, L. Lingstedt, P. Romele, N. I. Crăciun, Z. M. Kovács-Vajna, P. W. M. Blom, F. Torricelli, *Nat. Commun.* **2018**, 9, 1.
- [40] L. V. Lingstedt, M. Ghittorelli, M. Brückner, J. Reinholz, N. I. Crăciun, F. Torricelli, V. Mailänder, P. Gkoupidenis, P. W. M. Blom, *Adv. Healthcare Mater.* **2019**, 8, 1900128.
- [41] E. Cantatore, T. C. T. Geuns, G. H. Gelinck, E. van Veenendaal, A. F. A. Gruijthuijsen, L. Schrijnemakers, S. Drews, D. M. de Leeuw, *IEEE J. Solid-State Circuits* **2007**, 42, 84.



- [42] a) X. Y. Yu, B. H. Schofield, T. Croxton, N. Takahashi, E. W. Gabrielson, E. W. Spannake, *Am. J. Respir. Cell Mol. Biol.* **1994**, *11*, 188; b) X. Y. Yu, N. Takahashi, T. L. Croxton, E. W. Spannake, *Environ. Health Perspect.* **1994**, *102*, 1068.
- [43] a) M. González Ferreiro, G. H. L. G. Tillman, R. Bodmeier, *Pharm. Res.* **2002**, *19*, 755; b) Y. Fang, J. Xue, L. Ke, Y. Liu, K. Shi, *Drug Delivery* **2016**, *23*, 3582.
- [44] G. Sitterley, *BioFiles* **2008**, *3*, 12.
- [45] a) D. A. Volpe, *J. Pharm. Sci.* **2008**, *97*, 712; b) J. Reinholz, C. Diesler, S. Schöttler, M. Kokkinopoulou, S. Ritz, K. Landfester, V. Mailänder, *Acta Biomater.* **2018**, *71*, 432.
- [46] a) B. Christ, C. Fey, A. Cubukova, H. Walles, S. Dembski, M. Metzger, *Springer Sci.+Business Media LLC* **2017**, *1601*, 111; b) M. Fisichella, F. Berenguer, G. Steinmetz, M. Auffan, J. Rose, O. Prat, *BMC Genomics* **2014**, *15*, 1.